DOI: 10.1478/AAPP.1001A6

AAPP | Atti della Accademia Peloritana dei Pericolanti
Classe di Scienze Fisiche, Matematiche e Naturali
ISSN 1825-1242

Vol. 100, No. 1, A6 (2022)

SURFACE MODIFIED CARBON VULCAN BASED ELECTRODES FOR ELECTROCATALYTIC REDUCTION OF CO_2 TO HIGH VALUE PRODUCTS

GEORGIA PAPANIKOLAOU [a], DONATELLA CHILLÈ [a], PAOLA LANZAFAME [a], MARIA TERESA CACCAMO [b] * AND SALVATORE MAGAZÙ [b]

ABSTRACT. The electrocatalytic reduction of CO_2 (CO_2RR) in high value products represents a high potential strategy in addressing global climate change. Vulcan XC-72 carbon black is considered to be a promising catalyst support for metals nanoparticles in the CO_2RR due to its good electrical properties, high mesoporous distribution and low cost. In this work we reported how the surface chemical modification of Vulcan XC-72 carbon leads to the introduction of oxygenated functionalities with a significant increase of the activity in the electrocatalytic reduction of CO_2 to formic acid. The presence of oxygen-containing species results advantageous for the dispersion and anchoring of Sn nanoparticles onto carbon surface increasing the Faradaic selectivity to formic acid up to 80%.

1. Introduction

The electrocatalytic reduction of CO_2 (CO_2RR) represents a very promising strategy to close the anthropogenic carbon cycle allowing the storage of the fluctuating renewable energy (*e.g.*, solar and wind energy) in the form of chemicals and fuels (Perathoner and Centi 2018; G. Wang *et al.* 2021). Compared to other strategies, the electrocatalytic approach allows to operate at ambient pressure and temperature conditions and to control the products selectivity by applied potentials or current (Liu *et al.* 2020). Moreover, the electrocatalytic reactions avoid the use of fossil H_2, exploiting that derived from electrochemical water splitting reaction (Turner *et al.* 2008). The main challenge in achieving the aforementioned objective is the development of low-cost electrocatalysts with excellent selectivity and stability, particularly at high current densities. Carbon-based electrocatalysts in comparison to massive metal electrodes, show an enhanced activity which can be attributed to the better distribution of CO_2 on the active surface (Pérez-Rodríguez *et al.* 2017). Novel carbon structures like mesoporous carbons, graphene, carbon nanofibers and nanotubes are promising materials and studies related to their application as electrocatalysts for the electrochemical reduction of CO_2 are of growing interest (Messias *et al.* 2019). However, carbon blacks represent the most studied carbon materials for this purpose and play a key role for the intensification of electrochemical CO_2 reduction. Carbon blacks are commonly

applied supports for metal containing electrocatalysts (Genovese *et al.* 2015) due to their electrical properties, high surface area, low cost and possibility to be prepared in a large scale. Among the other different carbon blacks, Vulcan XC-72 carbon is receiving a great deal of attention as a catalyst support due to the high conductivity (~ 2.8 S·cm^{-1}) and the significant surface area (~ 250 m$^2 \cdot$ g^{-1}) (Tang *et al.* 2010).

Several metals have been supported on Vulcan carbon to obtain electrocatalysts for the electrochemical reduction of CO_2 to formic acid, a valuable building block with potential industrial applications in the textile manufacturing, as antibacterial and additive in the cement production. Mahmood et al. reported that CO_2 can be reduced to formic acid by using electrocatalysts based on Sn, In and Pb supported on Vulcan carbon (metal loading $\sim 50\%$ wt.), even if high loading of electrocatalysts on working electrode (from 50 to 100 mg·cm^{-2}) are needed to achieve current efficiency of about 80% (Mahmood *et al.* 1987). The use of Bi-Vulcan based electrodes leads to Faradaic efficiency of $\sim 100\%$ although the electrocatalyst deactivation due to the gradual loss of Bi was observed (Ávila-Bolívar *et al.* 2019). The weak interaction of the metal nanoparticles (NPs) with the carbon surface, as well as their poor dispersion, are prevalently due to the lack of oxygen functional groups on Vulcan surface, which results in an unstable electrocatalyst by cause of the leaching of the active phase (An *et al.* 2021; Papanikolaou *et al.* 2021).

One of the strategies used to improve the anchoring of the active phase on carbon surface is the introduction of oxygenated species on the carbon surface through oxidative treatments (Figueiredo *et al.* 1999). The surface modification of the carbon surface with carboxyls, carbonyls, quinones, lactones or phenols is advantageous not only for the dispersion and anchoring of the NPs but plays also an important role in the electrocatalytic behaviour (Rizo *et al.* 2017). In fact, the presence of oxygenated groups influences the surface polarity giving a hydrophilic character to the carbon surface, enhancing the capacitance and increasing the accessible surface area (Sanchez *et al.* 2017; Papanikolaou *et al.* 2022).

In this manuscript we address this issue through the introduction of oxygenated functionalities on Vulcan XC-72 by chemical oxidation treatment with concentrated nitric acid in order to stabilize Sn NPs on carbon surface. Del Castillo *et al.* (2017) reported that 70% of Faradaic efficiency to formic acid is reached by using an electrocatalyst based on 30% Sn NPs on Vulcan carbon, without any introduction of surface oxygenated functionalities. However, a high loading of electrocatalysts on working electrode is requested (Del Castillo *et al.* 2017). In our work Sn NPs were supported on oxygen functionalized Vulcan XC-72 via a wetting chemistry reduction method carbon in order to obtain electrocatalysts with a Sn loading of 5% wt. The textural and spectroscopic features of the obtained electrocatalysts were characterized by XRD, N_2 physisorption, FT-IR and Raman spectroscopy, SEM-EDX. The effect of the introduction of oxygenated functionalities on carbon was evidenced by studying their electrocatalytic activity in the CO_2RR under industrially relevant conditions. The results provide some interesting insights on the use of these functionalized materials as selective electrocatalysts for the conversion of CO_2 to formic acid.

2. Materials and methods

2.1. Preparation of electrocatalysts. Commercial carbon black (Vulcan XC-72) from Cabot Corporation USA, was used as starting material for the synthesis of the electrocatalysts. In order to introduce oxygenated functionalities on the surface, Vulcan XC-72 carbon was undergone to an oxidative treatment in concentrated HNO_3 (ACS reagent, 70%). 3 g of carbon material was treated in reflux at 110 °C for 3h in 150 mL afterwards the suspension was filtered and washed until neutral pH and dried at 80 °C for 12 hours. The sample obtained from this oxidative treatment is named $Vulcan_{ox}$. Tin metal NPs were deposited on Vulcan and functionalized Vulcan samples via a modified wetting chemistry reduction method with sodium citrate as a stabilizing agent and sodium borohydride as a reductive agent (Papanikolaou *et al.* 2019). The carbon support was suspended into an aqueous solution containing $SnSO_4$ (0.213 mmol, Sigma Aldrich) and sodium citrate (2mmol, Sigma Aldrich) and sonicated for 30 minutes. Afterwards, in the mixture was added drop by drop 25 mL of 0.1 M $NaBH_4$. The suspension was vigorously stirred for 5 h at room temperature. The Sn-based catalysts (indicated hereinafter as Sn@Vulcan and $Sn@Vulcan_{ox}$) were washed, filtered, dried at 80 °C for 12 h. The amount of Vulcan and $Vulcan_{ox}$ supports were calculated in order to obtain a final Sn loading of 5%wt.

2.2. Characterization of electrocatalysts. X-ray diffraction (XRD) data were collected by a Bruker D2 Phaser diffractometer equipped with a Cu tube ($\lambda = 1.54056$ Å) in the 2θ range of 12° – 80° with an angular step of 0.025 and acquisition rate of $1^\circ \cdot \text{min}^{-1}$. The textural properties were determined by adsorption/desorption isotherms of N_2 at 77 K (−196 °C) using a Quantachrome Autosorb iQ3 gas sorption analyser. Before the analysis all samples were degassed under vacuum at 300 °C for 2h in order to remove the possible impurities. Through the Brunauer-Emmett-Teller method was calculated the total surface area and the total pore volume by means of the single point method at $p/p^0 = 0.95$, instead the pore size distribution was determined using the BJH model considering the desorption branch of the N_2 isotherm. The surface morphology of the pristine carbon materials before and after the oxidative treatment was investigated by scanning electron microscopy (SEM) using a Phenom proX Desktop. For the energy dispersive X-rays (EDX) analysis, a higher voltage of 15 kV was applied in order to obtain the elemental composition of the samples through the production of the emission of X-rays from the samples. Raman spectroscopy was also performed by a DXR3xi Raman Imaging Microscope (Thermo Scientific) to determine the order of carbon materials after the oxidative treatment. The spectra were recorded using a laser excitation wavelength of 532 nm with a 10×0.25BN objective at room temperature for an exposure time of 180 s per spectrum. Raman peaks were deconvoluted using the Curve Fitting Program Peakfit V4 12 (Seasolve Software Inc). Fourier transform infrared (FT-IR) technique is a powerful experimental tool which allows to characterize the vibrational and rotational modes of a wide class of material systems. FT-IR typically covers the 14000-10 cm-1 spectral range of the electromagnetic spectrum. This wide spectral window is usually partitioned into three different sub-ranges, *i.e.*, the Near-IR (NIR) range, $14000 - 4000$ cm^{-1}, the Mid-IR (MIR) range, $4000 - 400$ cm^{-1}, and the Far-IR range, $400 - 10$ cm^{-1}. The spectrometer employed for the characterization of our systems is the Bruker Optics Alpha IR spectrometer, equipped with an ATR (Attenuated Total Reflectance) device which included a diamond window; spectra were acquired in the spectral region between 4000 and

400 cm^{-1} with a resolution of 4 cm^{-1}. In order to improve the signal-to-noise ratio, each spectrum was obtained by evaluating an average over 48 scans. Preprocessing data treatment was performed by using the Bruker OPUS/Mentor software. This included: i) a baseline treatment to diminish spectra dissimilarities due to baseline; ii) a smoothing treatment in order to reduce the instrumental noise; iii) a spectrum second derivative evaluation in order to better discriminate spectral features, with specific reference to band spectral frequencies. Data were analyzed by means of Mathematica and Matlab.

2.3. Fabrication of gas diffusion electrodes (GDE). For the fabrication of the gas diffusion electrodes (GDE), a gas diffusion layer (GDL, 29 BC Sigracet®) supplied by the fuelcellstore was employed and an ink contained the carbon based electrocatalyst was deposited onto gas diffusion layer by using an airbrush in order to obtain a homogeneous catalytic layer. The catalyst ink was prepared by suspending the carbon based materials in absolute Ethanol (99.8%) and adding 40 μL of a Nafion^{TM} perfluorinated resin (aqueous dispersion 10% wt.) solution under constant sonication for 30 minutes. The catalysts loading was determined by weighing the electrodes before and after the spraying thus obtaining a final loading of 0.5 $mg{\cdot}cm^{-2}$.

2.4. Electrochemical measurements. The electrochemical behaviour of all fabricated electrodes was studied in the electrocatalytic reduction of CO_2. For the electrocatalytic tests a Micro Flow Cell based on a three-electrode cell configuration (purchased from ElectroCell) was used. The fabricated electrodes with a surface of 10 cm^2 were used as working elettrodes (WE), instead a plan plate of Pt as anode, and a 1 mm leak-free Ag/AgCl (3.4 M KCl) electrode as a reference. The anolyte and the catholyte were separated by a proton exchange membrane Nafion® 115 (by Fuel Cell Store). For all the tests, 80 mL of 0.5 M Potassium bicarbonate ($KHCO_3$) solution was used as electrolyte divided equally into the two cathodic and anodic compartments. Through the use of a peristaltic pump, the electrolyte flow was kept constant at a value of 15 $mL{\cdot}min^{-1}$, instead the flow rate of CO_2 was 10 $mL{\cdot}min^{-1}$. The electrocatalytic tests were carried out in galvanostatic mode using for the power supply a potentiostat galvanostat (Autolab Pgstat 302n Metrohm) where each potential and current density was applied for 3h. The liquid products detection was performed using an 3D High-Performance Liquid Chromatography System (HPLC Shimadzu Nexera-I LC-2040C), equipped with an Aminex HPX-87H Column and a photo diode array (PDA) detector, while gas phase was analysed through an on-line Agilent 490 micro gas-chromatograph (Micro GC) equipped with a Molsieve 5 and a PoraPLOT Q columns.

3. Results and discussion

3.1. Structural and textural characterization. Figure 1a shows the XRD pattern of Vulcan XC-72 supports before (Vulcan) and after the oxidative treatment $Vulcan_{ox}$. For both samples it is possible to observe the highest intensity peak at $2\theta = 25°$corresponding at 002 crystal plane, characteristic of highly oriented pyrolytic graphite (HOPG). The diffraction angle (2θ) of the crystalline graphite is usually located at around 26.5°, this slight shift towards lower angle indicates that the Vulcan micro-crystallites differ from those of graphite (Lee *et al.* 2021). Moreover, both untreated and treated samples present also the diffraction

peak at above 43.6° corresponding to the 101 plane. Figure 1b reports the diffractograms after the deposition of Sn NPs where it is possible to observe the diffraction peaks for tetragonal metallic tin at 2θ = 30°, 32°, 44°, 45°, 55.3°, 62.6°, 63.8°, 64.6°, 64°, and 72.5°, 73.3° which correspond to the crystal planes of (200, 101, 220, 211, 301, 112, 400, 321) and (420, 411), respectively (JCPDS no.04–0673). The crystallite size of Sn NPs on Vulcan and $\text{Vulcan}_{\text{ox}}$ was determined through the Scherrer equation and was 36 nm and 26 nm, respectively.

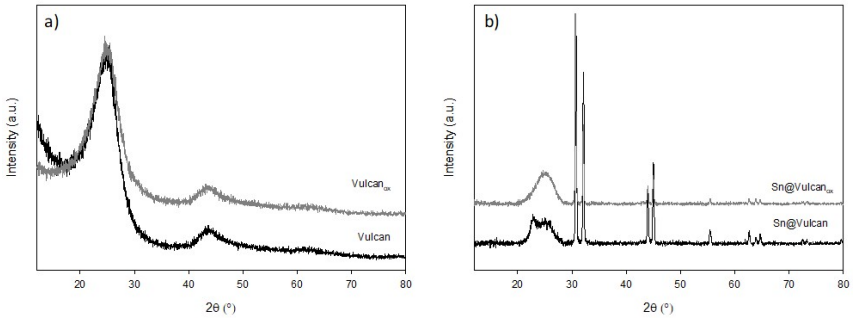

FIGURE 1. XRD patterns of Vulcan and $\text{Vulcan}_{\text{ox}}$ supports (a) and Sn@Vulcan and $\text{Vulcan}_{\text{ox}}$ (b).

The N_2 adsorption–desorption isotherms are reported in Fig. 2 where it is possible to observe that all Vulcan supports present a type IV isotherm with an H3 hysteresis, characteristic of slit-shaped pores, in line with the literature (Leofanti *et al.* 1998; Marsh and Rodríguez-Reinoso 2006), indicating the mesoporous texture of the samples. Moreover, the oxidative functionalization treatment does not affect the isotherms profile.

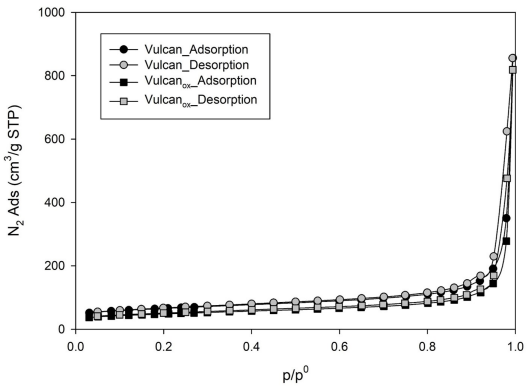

FIGURE 2. N_2 adsorption/desorption isotherms for Vulcan and $\text{Vulcan}_{\text{ox}}$ supports.

Table 1 summarizes the textural properties obtained for Vulcan supports before and after the oxidation treatment. The HNO_3 treatment of Vulcan sample leads to a marked decrease in the surface area (235 to 171.8 $m^2 \cdot g^{-1}$) with a consequent decrease in both the microporous area (95.9 to 62.2 $m^2 \cdot g^{-1}$) and volume (0.040 to 0.026 $cm^3 \cdot g^{-1}$), attributed to the partial collapse of the pore walls induced by the introduction of oxygen groups following the oxidative treatment (Pérez-Rodríguez *et al.* 2018).

TABLE 1. Texural properties of Vulcan and $Vulcan_{ox}$ supports.

Samples	SA_{BET}[a]	SA_{micro}[b]	SA_{ext}[b]	V_{pore}[c]	V_{micro}[b]	d_{pore}
	($m^2 \cdot g^{-1}$)			($cm^3 \cdot g^{-1}$)		(Å)
Vulcan	235.0	95.9	139.1	1.25	0.040	25
$Vulcan_{ox}$	171.8	62.2	109.6	1.21	0.026	26

[a] Specific Surface area, calculated using the BET method
[b] Calculated by the t-plot method
[c] Single point adsorption total pore volume measured at 0.95 p/p°

The morphology was investigated by SEM. Figure 3 reports the SEM images of pristine and surface modified Vulcan samples. No changes in the morphology of the samples can be observed indicating that the oxidative treatment did not modify significantly their morphology (Figs. 3a and 3b). Through an energy dispersive X-ray analysis (EDX) was possible to determine the atomic concentration of the elements present before and after the oxidation treatment. The analysis of the results evidences an increase in the atomic percentage of oxygen from 20% to 33% accompanied from a decrease in the C/O ratio varying from 4.1 to 2.0 for Vulcan and $Vulcan_{ox}$, respectively. Figure 4 shows the SEM

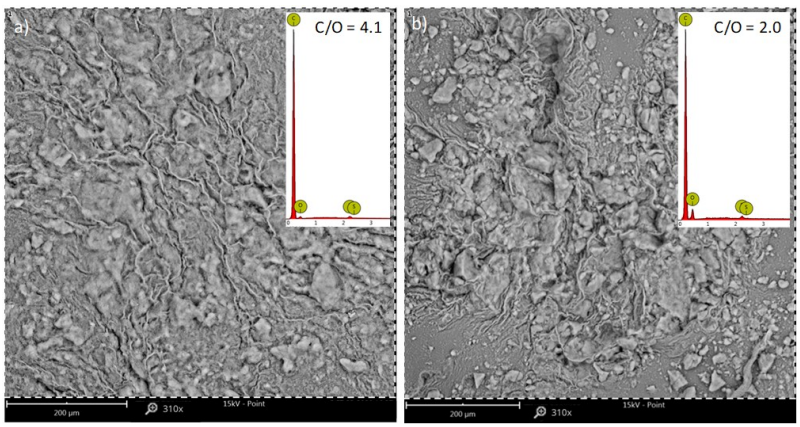

FIGURE 3. SEM micrographs of Vulcan (a) and $Vulcan_{ox}$ (b) and corresponding EDX spectra (inset).

image of Sn@$Vulcan_{ox}$ sample. It is possible to observe a highly degree of dispersion of

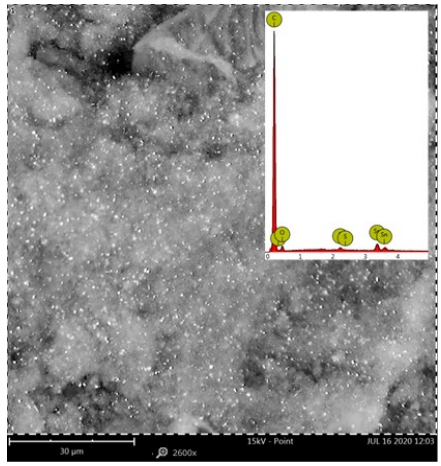

FIGURE 4. SEM micrograph of Sn@Vulcan$_{ox}$ and corresponding EDX spectra (inset).

the Sn NPs (lighter shaded particles). The elemental analysis for both Sn@Vulcan and Sn@Vulcan$_{ox}$ samples confirms the theoretical Sn loading of 5 %wt.

3.2. Spectroscopic characterization. In infrared (IR) spectroscopy spectra are measured by calculating the intensity of infrared radiation before and after it passes through a sample so detecting absorption peaks, connected with the system rotational and vibrational modes, whose band positions and intensity result intimately connected with the specific system chemical structures, with their population and with their dynamics. IR absorption spectroscopy is complementary to Raman scattering, to inelastic neutron scattering and to density function simulations, these techniques, with different sensitivities and different space-time scales, furnishing comparable information on the systems structural and dynamical properties (Caccamo and Magazù 2016; Magazù *et al.* 2018).

Figure 5 shows the comparison of FT-IR spectra of the Vulcan and Vulcan$_{ox}$ samples in the 1000 cm^{-1} – 2730 cm^{-1} spectral range while Fig. 6 shows the difference between the Vulcan and Vulcan$_{ox}$ properties. As far as the investigated spectral range is concerned, it can be divided into two parts: the first called the region of functional groups (from 2730 to 1500 cm^{-1}), the second called the fingerprint region (from 1500 to 1000 cm^{-1}). In order to extract quantitative information on the sample composition starting from the registered spectral features, we shall focus the attention on the bands centred at a wavelength of 1979 cm^{-1}, attributed to pure C modes, on the band centred at a wavelength of 1287 cm^{-1}, attributed to C-O modes, on the band centred at a wavelength of 1979 cm^{-1}, attributed to C=C=C modes, on the band centred at a wavelength of 2155 cm^{-1}, attributed to C=C=O modes, and on the band centred at a wavelength of 2439 cm^{-1}, attributed to O=C=O modes. In particular, assuming that the IR peak intensities are proportional to the number of absorbing atoms, we will extract information on the relative percentage composition of the investigated samples.

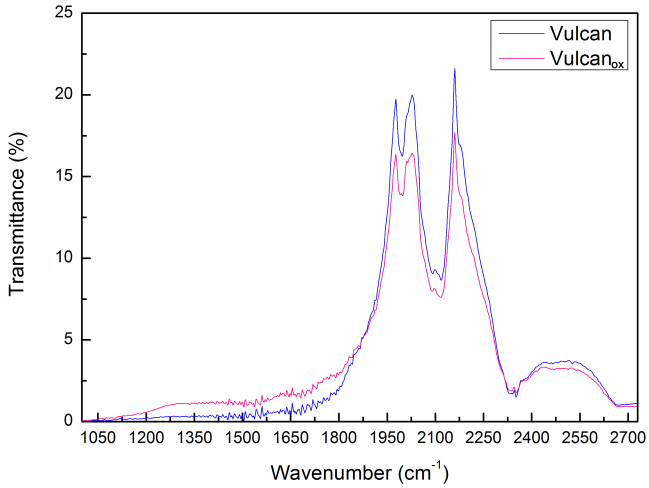

FIGURE 5. Comparison of FT-IR spectrum of Vulcan and Vulcan$_{ox}$ samples in the 1000 cm^{-1} – 2730 cm^{-1} spectral range.

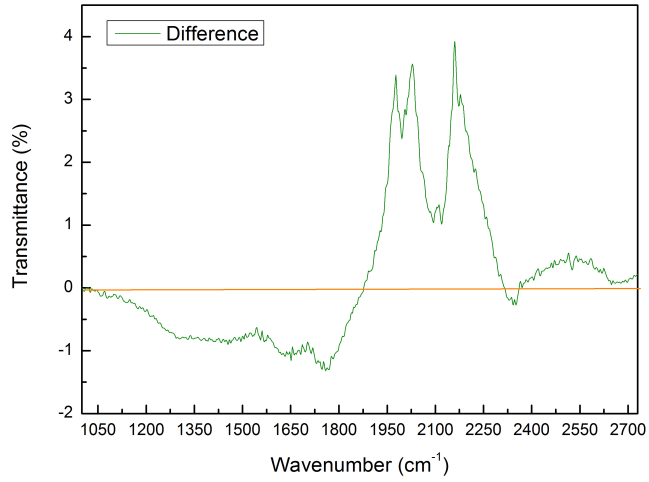

FIGURE 6. Difference between Vulcan and Vulcan$_{ox}$ spectra in the 1000 cm^{-1} – 2730 cm^{-1} spectral range.

Table 2 shows the center frequencies and the intensities of the peaks for the Vulcan and the $\text{Vulcan}_{\text{ox}}$ samples, together with the intensity ratios.

TABLE 2. Center frequencies and the intensities of the bands for the Vulcan and $\text{Vulcan}_{\text{ox}}$ supports together with the corresponding intensity ratios.

	IR peak frequency			
	1287 cm^{-1} (C-O)	**1979 cm^{-1} (C=C=C)**	**2155 cm^{-1} (C=C=O)**	**2439 cm^{-1} (O=C=O)**
Vulcan	0.33	19.20	18.05	3.62
$\text{Vulcan}_{\text{ox}}$	1.06	15.99	15.02	3.34
$I_{\text{Vulcan}}/I_{\text{Vulcan}_{\text{ox}}}$	0.31	1.20	1.20	1.08

The ratio between the IR intensity peaks, attributed to the C=C=C mode, centred at $\Delta\omega = 1979.31$ cm^{-1} for the two samples, *i.e.*, the Vulcan and $\text{Vulcan}_{\text{ox}}$, furnishes a value of $19.20/15.99 = 1.20$; the same intensity ratio $18.05/15.02 = 1.20$ is also obtained for the peaks, attributed to the C=C=O mode centred at $\Delta\omega = 2155$ cm^{-1}. On the other hand the ratio between the IR intensity peaks centred at $\Delta\omega = 1287$ cm^{-1}, attributed to the C-O mode, for the two samples, *i.e.*, the Vulcan and $\text{Vulcan}_{\text{ox}}$ samples, furnishes a value of $0.33/1.06 = 0.31$, whereas the ratio of the intensity peaks centred at 2439 cm^{-1}, attributed to the O=C=O mode, is $3.62/3.34 = 1.08$. These findings confirm the composition analysis extracted by EDX which reveals a significant decrease in the C/O ratio. On the other hand, by taking the average between the intensity ratios of the C-O and O=C=O modes we obtain a value of 0.69 which agrees quite well with the Oxygen percentage of the Vulcan O (20%) and of $\text{Vulcan}_{\text{ox}}$ sample O (33%), *i.e.*, $O_{\text{Vulcan}}/O_{\text{Vulcan}_{\text{ox}}} = 0.60$.

Raman spectroscopy is widely used for the characterization of carbon based materials and in particular for the determination of the degree of order or disorder of the structure (Bokobza *et al.* 2014). The Raman recorded spectra of pristine and surface modified Vulcan XC-72 samples are reported in Fig. 7.

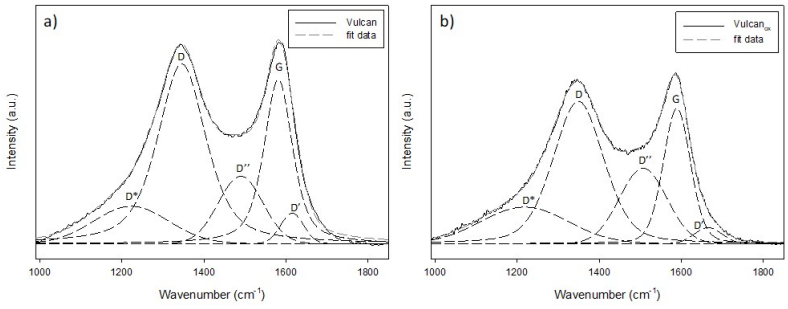

FIGURE 7. Five functions (D^*, D, D'', G, and D' bands) deconvolution of Raman spectra for Vulcan and $\text{Vulcan}_{\text{ox}}$ supports.

The spectra show the D and G band located at around 1350 cm^{-1} and 1580 cm^{-1}, respectively. The D band is due to the presence of a structural disorder originate from a hybridized vibrational mode to the graphene edges. It indicates the presence of amorphous carbon and defects in the structure (Schüpfer *et al.* 2020). The G band is due to the graphitic structure originates from the E2g vibration mode representing the sp2 bonded carbons. The intensity ratio of the D to G band allows to obtain useful information on the defect density of the carbon materials. However, in order to avoid an erroneous evaluation of the degree of order through the I_D/I_G ratio, it is also necessary to take into account the additional contributions of the bands obtained from D and G bands deconvolution. In fact, if the contribution of these additional bands is not considered, the estimation of the degree order could be inaccurate, due to the bands superposition, especially in presence of a highly defective structure. We identified and calculated the contribution of the D^*, D'', and D' bands through the combination and fitting of five Lorentzian/Gaussian functions. The D* band is located around 1250 cm^{-1} and its presence is due to the vibration of sp3 hybridized carbons which are bonded to oxygen-containing groups. The D'' band at 1500 cm^{-1} is associated to the decrease of crystallinity (Vollebregt *et al.* 2012). The D' band observed at 1620 cm^{-1} is attributed to sp2 nanostructures with a strained geometry (Groppo *et al.* 2018). Following the oxidative treatment an increase of the I_D/I_G is observed, passing from 1.81 for Vulcan to 1.99 for $Vulcan_{ox}$, due to the decrease of order degree. The increase of the I_{D^*}/I_G ratio from 0.48 for Vulcan to 0.79 for $Vulcan_{ox}$ sample also confirms the introduction of the oxygenated groups on carbon surface bonded to C sp3 atoms. The $I_{D''}/I_G$ is related to the presence of amorphous carbon and provides additional information regarding the crystallinity of the carbon materials. The analysis of the $I_{D''}/I_G$ ratio evidences an increase of the ratio which increases from 0.52 (Vulcan) to 0.89 ($Vulcan_{ox}$), indicating a partial amorphization induced by the oxidative treatment. This result is in line with the net decrease of surface area, associated to the partial collapse of the carbon structure induced by the introduction of oxygen groups (Pérez-Rodríguez *et al.* 2018).

3.3. Electrocatalytic activity. Sn@Vulcan and $Sn@Vulcan_{ox}$ electrocatalysts were used for the fabrication of working electrodes and tested in CO_2RR using a Micro Flow Cell based on a three-electrode cell configuration under industrially relevant conditions (high current 100 mA). The prepared electrodes were tested for 3 h and the electrocatalytic performances were compared with those of the metal-free supports. For all samples the main product detected in liquid phase was formic acid, instead H_2, formed through the competitive hydrogen evolution reaction (HER) was revealed in the gas phase.

Figure 8 shows the production of formic acid for all fabricated working electrodes along 3 h of reaction. By comparing the results obtained using metal-free Vulcan and $Vulcan_{ox}$, it is possible to evidence how the modification of the carbon surface by introduction of oxygen functionalities, evidenced by the FT-IR and Raman spectroscopic characterization, leads to an increase of formic acid production, which reaches for metal-free $Vulcan_{ox}$ a value of 1.5 times higher than unmodified Vulcan after 3 h of reaction. This behaviour can be attributed to the higher wettability of the modified support which favours the diffusion of CO_2 through the carbon based working electrode. The introduction of Sn NPs increases significantly the formic acid production for both Vulcan and $Vulcan_{ox}$ support, observing the highest productivity for $Sn@Vulcan_{ox}$.

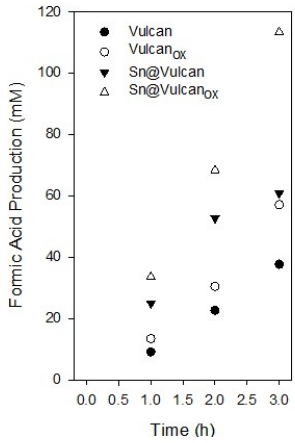

FIGURE 8. Production of formic acid formation over the time.

Another aspect to highlight is the trend of formic acid formation along the time, strictly correlated to the stability of the catalyst. For Sn@Vulcan$_{ox}$, the production of formic acid increases exponentially with the time up to a concentration of 113 mM, whereas Sn@Vulcan reaches a plateau at about 56 mM (Fig. 8). This behaviour can be attributed to the higher dispersion and stabilization of the Sn NPs on the modified Vulcan$_{ox}$, also evidenced by EDX analysis, probably due the improved anchoring by –COOH groups on the surface of the support (Lanzafame *et al.* 2007) thus limiting the leaching of the active phase.

Table 3 reports the value of Faradaic efficiency towards formic acid after 3 h of reaction. The analysis of Faradaic efficiency is of fundamental importance in the electrocatalytic field because this parameter describes the efficiency with which the electrons are transferred in a reagent system facilitating the selective electrochemical formation of a specific product.

TABLE 3. Faradaic efficiency to formic acid and H_2 evolution (100 mA, 3 h) and CO_2RR products distribution.

Samples	FE to formic acid %	H_2 evolution %
Vulcan	26.0	5.5
Vulcan$_{ox}$	40.8	6.4
Sn@Vulcan	35.6	3.9
Sn@Vulcan$_{ox}$	80.9	2.2

It is possible to observe that the Faradaic efficiency to formic acid for unmodified metal-free Vulcan is 26%, after oxidative treatment $Vulcan_{ox}$ reaches a higher value of more than 1.5 times (40.8%). The Faradaic efficiency increase significantly after the dispersion of Sn NPs, reaching a value of 80.9% for the surface modified $Sn@Vulcan_{ox}$. This enhancement of the electrocatalytic perfomances support the hypothesis that the more hydrophilic character of the Vulcan support induced by the presence of oxygen functionalities on the surface, improves the wettability of the electrocatalyst (Shi *et al.* 2020) favouring the diffusion of CO_2 to the active sites (Ghosh *et al.* 2020; Zou and S. Wang 2021). Along the time of reaction, no significant variation of the potential was observed for all electrocatalysts. The highest value of potential (~ -1.9 V vs Ag/AgCl) was measured for both metal-free Vulcan electrodes associated with a major H_2 evolution. On the other hand, the potential measured for Sn@Vulcan remains constant at -1.8 V vs Ag/AgCl, whereas the minor value was observed for $Sn@Vulcan_{ox}$ (-1.7 V vs Ag/AgCl) for which an inhibition of the competitive H_2 evolution reaction is observed, as evidenced by the lowest amount of H_2 revealed in the gas phase.

4. Conclusions

The electrocatalytic performances of Vulcan based electrocatalysts in the CO_2RR to formic acid, a valuable building block with a wide range of industrial applications, was remarkably improved by covalent modification of the carbon support based on surface oxidation. The introduction of oxygen functionalities increases the polarity of the Vulcan XC-72 carbon black improving the diffusion of CO_2 through the carbon based electrode, leading to an enhancement of the activity towards formic acid for metal-free surface functionalized $Vulcan_{ox}$ 1.5 times higher than unmodified Vulcan. This result is of potential interest for the development of metal free carbon based electrocatalysts with low cost. The functionalization of the Vulcan surface allows a better dispersion and anchoring of the Sn NPs leading to a more stable electrocatalyst with a significantly enhanced selectivity to formic acid of 80.9%.

Acknowledgments

This work was realized in the frame of the project PON-AIM "Attraction and International Mobility I.1 -I.2" (CUP J44I180 0 0140 0 06 − CUP J44I180 0 0130 0 06).

References

An, L., Wei, C., Lu, M., Liu, H., Chen, Y., Scherer, G., Fisher, A., Xi, P., Xu, Z., and Yan, C.-H. (2021). "Recent development of oxygen evolution electrocatalysts in acidic environment". *Advanced Materials* **33**(20), 2006328. DOI: 10.1002/adma.202006328.

Ávila-Bolívar, B., Garcia-Cruz, L., Montiel, V., and Solla-Gullon, J. (2019). "Electrochemical Reduction of CO_2 to Formate on Easily Prepared Carbon-Supported Bi Nanoparticles". *Molecules* **24**, 2032–2046. DOI: 10.3390/molecules24112032.

Bokobza, L., Bruneel, J.-L., and Couzi, M. (2014). "Raman spectroscopy as a tool for the analysis of carbon-based materials (highly oriented pyrolitic graphite, multilayer graphene and multiwall carbon nanotubes) and of some of their elastomeric composites". *Vibrational Spectroscopy* **74**, 57–63. DOI: 10.1016/j.vibspec.2014.07.009.

Caccamo, M. T. and Magazù, S. (2016). "Tagging the oligomer-to-polymer crossover on EG and PEGs by infrared and Raman spectroscopies and by wavelet cross-correlation spectral analysis". *Vibrational Spectroscopy* **85**, 222–227. DOI: 10.1016/j.vibspec.2016.04.017.

Del Castillo, A., Alvarez-Guerra, M., Solla-Gullón, J., Sáez, A., Montiel, V., and Irabien, A. (2017). "Sn nanoparticles on gas diffusion electrodes: Synthesis, characterization and use for continuous CO_2 electroreduction to formate". *Journal of CO_2 Utilization* **18**, 222–228. DOI: 10.1016/j.jcou.2017.01.021.

Figueiredo, J., Pereira, M., Freitas, M., and Orfao, J. J. (1999). "Modification of the Surface Chemistry of Activated Carbon". *Carbon* **37**, 1379–1389. DOI: 10.1016/S0008-6223(98)00333-9.

Genovese, C., Ampelli, C., Marepally, B., Papanikolaou, G., Perathoner, S., and Centi, G. (2015). "Electrocatalytic reduction of CO_2 for the production of fuels: A comparison between liquid and gas phase conditions". *Chemical Engineering Transactions* **43**, 2281–2286. DOI: 10.3303/CET1543381.

Ghosh, S., Barg, S., Jeong, S. M., and Ostrikov, K. (2020). "Heteroatom-Doped and Oxygen-Functionalized Nanocarbons for High-Performance Supercapacitors". *Advanced Energy Materials* **10**, 2001239 [44 pages]. DOI: 10.1002/aenm.202001239.

Groppo, E., Bonino, F., Cesano, F., Damin, A., and Manzoli, M. (2018). "Raman, IR and INS Characterization of Functionalized Carbon Materials". In: *Metal-free Functionalized Carbons in Catalysis: Synthesis, Characterization and Applications*. Ed. by N. D. Alberto Villa. Cambridge: RSC Catalysis Series. Chap. 4, pp. 105–137. DOI: 10.1039/9781788013116-00103.

Lanzafame, P., Perathoner, S., Centi, G., and Frusteri, F. (2007). "Synthesis and characterization of Co-containing SBA-15 catalysts". *Journal of Porous Materials* **14**, 305–313. DOI: 10.1007/s10934-006-9068-0.

Lee, S.-M., Lee, S.-H., and Roh, J.-S. (2021). "Analysis of Activation Process of Carbon Black Based on Structural Parameters Obtained by XRD Analysis". *Crystals* **11**, 153–163. DOI: 10.3390/cryst11020153.

Leofanti, G., Padovan, M., Tozzola, G., and Venturelli, B. (1998). "Surface Area and Pore Texture of Catalysts". *Catalysis Today* **41**, 207–219. DOI: 10.1016/S0920-5861(98)00050-9.

Liu, A., Gao, M., Ren, X., Meng, F., Yang, Y., Gao, L., Yang, Q., and Ma, T. (2020). "Current progress in electrocatalytic carbon dioxide reduction to fuels on heterogeneous catalysts". *Journal of Materials Chemistry A* **8**, 3541–3562. DOI: 10.1039/C9TA11966C.

Magazù, S., Calabrò, E., and Caccamo, M. T. (2018). "Experimental study of thermal restraint in bio-protectant disaccharides by FTIR spectroscopy". *The Open Biotechnology Journal* **12**, 123–133. DOI: 10.2174/1874070701812010123.

Mahmood, M. N., Masheder, D., and Harty, C. J. (1987). "Use of gas-diffusion electrodes for high-rate electrochemical reduction of carbon dioxide. I. Reduction at lead, indium- and tin-impregnated electrodes". *Journal of Applied Electrochemistry* **17**, 1159–1170. DOI: 10.1007/BF01023599.

Marsh, H. and Rodríguez-Reinoso, F. (2006). *Activated Carbon*. Elsevier Science Ltd. DOI: 10.1016/B978-0-08-044463-5.X5013-4.

Messias, S., Nunes da Ponte, M., and S. Reis-Machado, A. (2019). "Carbon Materials as Cathode Constituents for Electrochemical CO_2 Reduction–A Review". *C – Journal of Carbon Research* **5**(4), 83 [26 pages]. DOI: 10.3390/c5040083.

Papanikolaou, G., Chillè, D., Abate, S., Perathoner, S., Centi, G., Giorgianni, G., Cozza, D., Dalena, F., Migliori, M., Giordano, G., and Lanzafame, P. (2022). "Zeolite templated carbon from Beta replica as metal-free electrocatalyst for CO_2 reduction". *Applied Materials Today* **26**, 101383 [13 pages]. DOI: 10.1016/j.apmt.2022.101383.

Papanikolaou, G., Lanzafame, P., Giorgianni, G., Abate, S., Perathoner, S., and Centi, G. (2019). "Highly selective bifunctional Ni zeo-type catalysts for hydroprocessing of methyl palmitate to green diesel". *Catalysis Today* **345**, 14–21. DOI: 10.1016/j.cattod.2019.12.009.

Papanikolaou, G., Lanzafame, P., Perathoner, S., Centi, G., Cozza, D., Giorgianni, G., Migliori, M., and Giordano, G. (2021). "High performance of Au/ZTC based catalysts for the selective oxidation of bio-derivative furfural to 2-furoic acid1". *Catalysis Communications* **149**, 106234 [6 pages]. DOI: 10.1016/j.catcom.2020.106234.

Perathoner, S. and Centi, G. (2018). "Catalysis for solar-driven chemistry: The role of electrocatalysis". *Catalysis Today* **330**, 157–170. DOI: 10.1016/j.cattod.2018.03.005.

Pérez-Rodríguez, S., Pastor, E., and Lázaro, M. J. (2018). "Electrochemical behavior of the carbon black Vulcan XC-72R: Influence of the surface chemistry". *International Journal of Hydrogen Energy* **43**, 7911–7922. DOI: 10.1016/j.ijhydene.2018.03.040.

Pérez-Rodríguez, S., Sebastián, D., Lazaro, M. J., and Pastor, E. (2017). "Stability and catalytic properties of nanostructured carbons in electrochemical environments". *Journal of Catalysis* **355**, 156–166. DOI: 10.1016/j.jcat.2017.09.019.

Rizo, R., Sebastian, D., Rodríguez, J. L., Lazaro, M. J., and Pastor, E. (2017). "Influence of the nature of the carbon support on the activity of Pt/C catalysts for ethanol and carbon monoxide oxidation". *Journal of Catalysis* **348**, 22–28. DOI: 10.1016/j.jcat.2017.02.007.

Sanchez, A., Izquierdo, M. T., Mathieu, S., Gonzalez-Alvarez, J., Celzard, A., and Fierro, V. (2017). "Outstanding electrochemical performance of highly N- and O-doped carbons derived from pine tannin". *Green Chemistry* **19**, 2653–2665. DOI: 10.1039/C7GC00491E.

Schüpfer, D., Badaczewski, F., Guerra-Castro, J., Hofmann, D., Heiliger, C., Smarsly, B., and Klar, P. (2020). "Assessing the structural properties of graphitic and non-graphitic carbons by Raman spectroscopy". *Carbon* **161**, 359–372. DOI: 10.1016/j.carbon.2019.12.094.

Shi, R., Guo, J., Xuerui, Z., Waterhouse, G., Han, Z., Yunxuan, Z., Shang, L., Zhou, C., Jiang, L., and Zhang, T. (2020). "Efficient wettability-controlled electroreduction of CO_2 to CO at Au/C interfaces". *Nature Communications* **11**, 3028 11 pages. DOI: 10.1038/s41467-020-16847-9.

Tang, S., Sun, G., QI, J., Sun, S., Guo, J., Xin, Q., and Haarberg, G. M. (2010). "Review of New Carbon Materials as Catalyst Supports in Direct Alcohol Fuel Cells". *Chinese Journal of Catalysis* **31**, 12–17. DOI: 10.1016/S1872-2067(09)60034-6.

Turner, J., Sverdrup, G., Mann, M., Maness, P.-C., Kroposki, B., Ghirardi, M., Evans, R., and Blake, D. (2008). "Renewable Hydrogen Production". *International Journal of Energy Research* **32**, 379–407. DOI: 10.1002/er.1372.

Vollebregt, S., Ishihara, R., Tichelaar, F. D., Hou, Y., and Beenakker, C. I. (2012). "Influence of the growth temperature on the first and second-order Raman band ratios and widths of carbon nanotubes and fibers". *Carbon* **50**, 3542–3554. DOI: 10.1016/j.carbon.2012.03.026.

Wang, G., Chen, J., Ding, Y., Cai, P., Luocai, Y., Yan, L., Tu, C., Hou, Y., Wen, Z., and Dai, L. (2021). "Electrocatalysis for CO_2conversion: From fundamentals to value-added products". *Chemical Society Reviews* **50**, 4993–5061. DOI: 10.1039/D0CS00071J.

Zou, Y. and Wang, S. (2021). "An Investigation of Active Sites for electrochemical CO_2 Reduction Reactions: From In Situ Characterization to Rational Design". *Advanced Science* **8**, 2003579 [20 pages]. DOI: 10.1002/advs.202003579.

[a] Università degli Studi di Messina,
Dipartimento di Scienze Chimiche, Biologiche, Farmaceutiche ed Ambientali,
Viale F. Stagno d'Alcontres, 98166 Messina, Italy

[b] Università degli Studi di Messina,
Dipartimento di Scienze Matematiche e Informatiche, Scienze Fisiche e Scienze della Terra,
Viale F. Stagno d'Alcontres, 98166 Messina, Italy

* To whom correspondence should be addressed | email: mcaccamo@unime.it

Communicated 26 November 2020; manuscript received 11 February 2022; published online 18 May 2022